

Long-distance measurement-device-independent quantum key distribution using entangled states between continuous and discrete variables

Soumyakanti Bose,^{1,*} Jaskaran Singh,^{2,†} Adán Cabello,^{2,3,‡} and Hyunseok Jeong^{1,§}

¹*Department of Physics & Astronomy, Seoul National University, Gwanak-ro 1, Gwanak-gu, Seoul 08826, Korea*

²*Departamento de Física Aplicada II, Universidad de Sevilla, E-41012 Sevilla, Spain*

³*Instituto Carlos I de Física Teórica y Computacional, Universidad de Sevilla, E-41012 Sevilla, Spain*

We introduce a feasible scheme to produce high-rate long-distance entanglement which uses hybrid entanglement (HE) between continuous variables (CV) and discrete variables (DV). We show that HE can effectively remove the experimental limitations of existing CV and DV measurement-device-independent quantum key distribution (MDI-QKD) protocols. The key idea is using the CV part, which can be adjusted to be robust against photon losses, for increasing the transmission distance, while using the DV part for achieving high secure key rates. We show that, using HE states, MDI-QKD is possible with standard telecom fibers for 300 km with a secure key rate which is an order of magnitude higher than in existing protocols. Our results point out that HE states provide advantage for practical long-distance high-rate entanglement.

Introduction.—Generation of high-rate entanglement between distant locations is crucial for fundamental tests of quantum theory and many applications. For example, it is needed for extending the current distances and rates of loophole-free Bell tests [1, 2], quantum steering [3], and quantum teleportation [4], which so far are only feasible for relatively short ranges. It is also needed for increasing the transmission distance and the key rate of entanglement-based quantum key distribution (QKD) protocols, most notably device-independent QKD [5–7], which currently suffers from both these issues. Moreover, higher-rates in distant locations will also allow us to achieve higher detection efficiencies (which are needed both for loophole-free Bell tests and device-independent QKD) by means of heralded qubit amplifiers [8] or photonic precertification schemes [9–11], whose practicality is currently limited by the rates achieved after transmission.

A benchmark of high-rate entanglement over long distances can be set by their performance in entanglement-based QKD protocols. More specifically, measurement-device-independent (MDI) QKD protocols [12–18] are of particular interest as they can effectively double the distance over which entanglement can be shared, while also providing a good secure key rate. Currently, MDI-QKD protocols can potentially share entanglement up to 220 kms with a key rate of the order of 10^{-10} bits per pulse using telecommunication wavelength and standard optical fibres [12, 19, 20]. MDI-QKD protocols are suitable for secure multiuser networks [21, 22] and have been experimentally demonstrated [19, 20, 23]. Moreover, they are an excellent test bed to efficiently generate and study entanglement between distant locations and in networks.

There are two types of MDI-QKD protocols: those that use discrete variable (DV) systems and those that

use continuous variable (CV) systems. For long-distance MDI-QKD, each type has its own set of advantages and limitations [24, 25]. As an example, DV-MDI-QKD protocols offer composable security proofs with good key rate. However, they require costly single-photon-sources and precise Bell-state or single-photon measurements, which are hard to perform even in laboratory conditions. On the other hand, CV-MDI-QKD protocols generally require Gaussian states which are comparatively easier to prepare, are robust against transmission losses, and can share entanglement over long distances. However, their performance is limited by the requirement of almost ideal homodyne detectors at telecommunication wavelength [17, 18]. As a consequence, despite an extensive theoretical and experimental analysis on both types of systems, the quest for an optimal physical system to share high-rate entanglement among distant parties remains open.

Nonetheless, there exists a different class of physical systems formally known as hybrid entangled (HE) states [26–30]. These strongly correlated [31–33] cross-system entangled states play a crucial role in various quantum information processing tasks, including quantum computation, communication, and tests of Bell non-locality [33–41], and have been efficiently generated in a wide range of experimental setups [42–46]. Consequently, using these states, it is possible to share entanglement among distant locations without the limitations faced by CV and DV systems.

In this Letter, we propose a scheme based on HE states as initial resource which produces high-rate entanglement between extremely far apart locations and thus can be efficiently used to generate secure keys. By bringing forth the best of both CV and DV systems in HE states, we show that it is possible to share entanglement and achieve secure key rate at a distance of 300 km by using practical homodyne detectors with efficiency $\eta_h = 0.55$ [47–51] (which is a reasonable value at telecom wavelengths [48]) and on-off detectors with efficiency $\eta_0 = 0.8$ [52], thereby surpassing earlier results

* soumyakanti.bose09@gmail.com

† jaskaran@us.es

‡ adan@us.es

§ h.jeong37@gmail.com

at telecommunication wavelengths on standard optical fibres. We also show that the key rate is an order of magnitude higher than previously reported [12], which is reflective of the quality of the correlations shared.

Our scheme hinges on generating a single-photon DV entangled state between two distant parties by exploiting CV entanglement swapping by a third party located midway. It offers three major advantages as compared to earlier CV and DV-MDI-QKD protocols. These are: (i) Elimination of major limiting factors of DV-MDI-QKD, which include high precision Bell state or single-photon measurements as well as the photon-number-splitting attack by an eavesdropper by considering entanglement swapping over the CV system. (ii) Elimination of the requirement of near-unit efficiency for the homodyne detectors used for key generation in CV-MDI-QKD. (iii) Long transmission distance at telecommunication wavelength stemming from the robustness of the multiphoton coherent state against transmission losses. Our scheme clearly exhibits the applicability and the importance of HE states in generating high-rate high-quality entanglement over 300 kms using realistic and widely available equipment.

Hybrid entangled states.—Let $|0\rangle$ and $|1\rangle$ correspond to photon number states in the Fock basis and $|\alpha\rangle$ correspond to a coherent state of a quantized light with coherent amplitude α . For the remainder of this paper we will represent the number of photons as a DV system, while the coherent state represents a CV system. We define a HE state as an entangled pair, where the entanglement is between the DV and CV degrees of freedom. Mathematically, such HE states can be written as

$$|\psi\rangle_{a_1 a_2} = \frac{1}{\sqrt{2}} (|0\rangle_{a_1} |\alpha\rangle_{a_2} + |1\rangle_{a_1} |-\alpha\rangle_{a_2}), \quad (1)$$

where a_1 and a_2 are the two modes pertaining to the DV and CV parts, respectively. We stress that HE states with small coherent amplitudes ($\alpha \lesssim 1$) are experimentally available. They have been generated experimentally using photon addition technique and a coherent state [42] as well as photon subtraction on two squeezed states [43] (see Appendix A for further detail). While these techniques produce HE states with non-unit probability, it should be noted that typical methods to generate standard entangled photon pairs, *e.g.*, the parametric down conversion, also does so non-deterministically.

Protocol.—We consider two distant parties, Alice and Bob, each of them having access to bipartite HE states $|\psi\rangle_{a_1 a_2}$ and $|\psi\rangle_{b_1 b_2}$ given by Eq. (1). We consider these as initial resource states which will be used to share a DV entangled state between the parties. We provide a step-by-step description of the protocol, schematically represented in Fig. 1, while a detailed mathematical calculation can be found in Appendix B.

Step 1: Alice and Bob generate HE states $|\psi\rangle_{a_1 a_2}$ and $|\psi\rangle_{b_1 b_2}$ in their respective laboratories. Both parties transmit the CV part of their systems, corresponding to modes a_2 and b_2 , respectively, to a third untrusted party,

Charlie, who lies midway between them, through a lossy quantum channel with transmittance T ($0 \leq T \leq 1$). Additionally, Bob also transmits the state $|\sqrt{2}\alpha\rangle$ to Charlie separately through a similar quantum channel. After passing through noisy channels, Charlie receives the mode a_2 from Alice, the mode b_2 from Bob, and the additional state $|\sqrt{2T}\alpha\rangle$ from Bob, which we label by mode c .

Step 2: Charlie mixes the two incoming modes a_2 and b_2 via a beam splitter (BS), labelled as BS_1 in Fig. 1 with two output modes which we can label as a'_2 and b'_2 . In our protocol we are specifically interested in the vacuum state contributions from the mode a'_2 . To extract this contribution, Charlie mixes this mode through a second BS (BS_2) with mode c with output modes labelled as a''_2 and c' . Charlie now performs a projective measurement, $\mathcal{M} = \{\Pi_0, \mathbb{1} - \Pi_0\}$, where $\Pi_0 = (\mathbb{1} - |0\rangle\langle 0|)_{a''_2} \otimes (\mathbb{1} - |0\rangle\langle 0|)_{c'}$. This measurement is accomplished by using on-off detectors (that only detect the presence of photons) on each of the modes a''_2 and c' . Charlie then publicly announces the outcome of the projective measurement which is considered to be successful only if the result Π_0 is obtained, *i.e.*, both detectors click. In that case, the protocol continues. Otherwise, the measurement is deemed unsuccessful and the parties must repeat the aforementioned steps again. In order to model realistic detectors, we consider imperfect on-off detectors with efficiency η_0 .

Step 3: After a successful projective measurement (as dictated in Step 2), Charlie performs a homodyne measurement on the mode b'_2 and, again, announces the results publicly. We consider that homodyne measurements have efficiency η_h .

Step 4: After a public announcement of the results of a successful projective measurement and the homodyne measurement by Charlie, Alice and Bob end up with the final normalized single-photon-Bell-state in modes a_1 and b_1 as (Appendix B 3)

$$\rho_{a_1 b_1} = \frac{1}{2} \left[|01\rangle\langle 01| + |10\rangle\langle 10| + f \left(g |01\rangle\langle 10| + g^* |10\rangle\langle 01| \right) \right] \quad (2)$$

with probability

$$p_0 = \frac{\left(1 - e^{-\eta_0 T \alpha^2} \right)^2}{2}, \quad (3)$$

where $f = e^{-4(1-T\eta_h)\alpha^2}$, $g = e^{4i\sqrt{T\eta_h}\alpha p}$, g^* is the conjugate of g , and p is the result of the homodyne measurement.

Step 5: For the case in which Alice and Bob share $\rho_{a_1 b_1}$, they perform two-outcome measurements \mathcal{M}_A and \mathcal{M}_B on their respective subsystems to generate a raw key. The choice of measurements is made prior to starting the protocol and the information about this choice is usually publicly available. In our protocol, they perform Pauli measurements corresponding to σ_Z on their respective

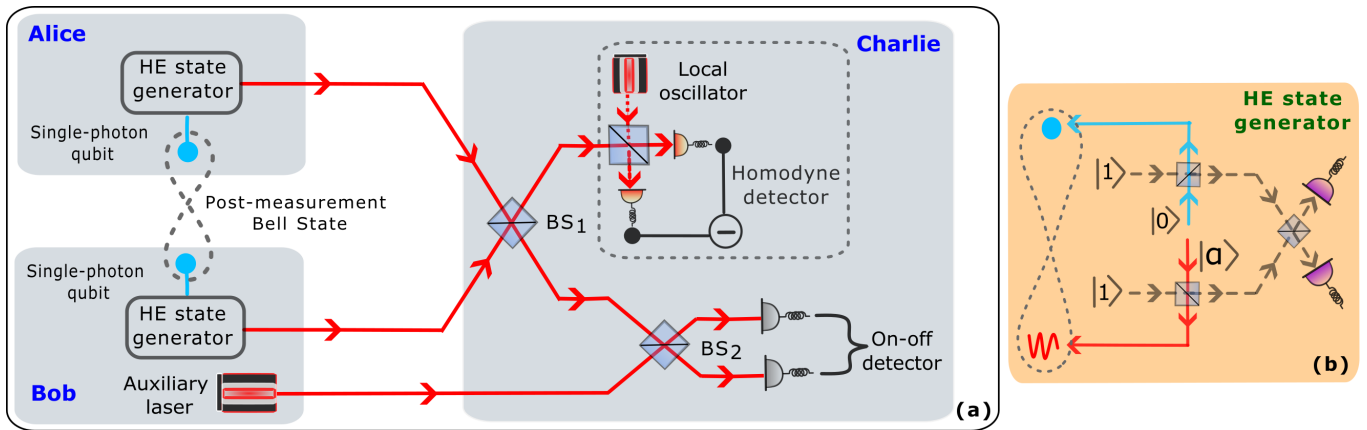


FIG. 1. (a) Scheme for generating DV entangled states between Alice and Bob using HE states. The DV part (cyan) and the CV part (red) of the HE state stand for the single-photon state and coherent state, respectively. Alice and Bob send the CV part of their individual HE states to Charlie, who then mixes the incoming signals at a balanced beam splitter (BS₁), and uses one of the output modes for homodyne measurement with efficiency η_h . The other outgoing signal of BS₁ is used for a post-selection measurement by on-off detectors with efficiency η_0 , after mixing it at another balanced BS (BS₂) with the additional coherent signal sent by Bob. Upon declaration of the results by Charlie, Alice and Bob obtain a DV entangled pair which is used for secure key generation. (b) Scheme for generating HE states. Two ancilla single photons (gray, dashed line) are mixed with vacuum and coherent states at the two BSs. The outgoing ancilla photons are then mixed with each other at a second BS. When the detector placed at the output of the second BS clicks, then the HE state between single-photon and the coherent state is obtained.

subsystems to generate a raw key. The length of the raw key that the parties can generate is quantified by the mutual information $I(A : B)$ between them for the observable σ_Z .

Step 6: Alice and Bob then estimate the amount of information that an adversary, Eve, can have on their raw key. This information is quantified by the Holevo bound $\chi(A : E)$ between Alice and Eve. In our protocol we consider the Holevo bound instead of quantum bit error rate (which is standard in DV-MDI-QKD protocols), because the knowledge about the coherent amplitude α , results of the on-off and homodyne measurement are publicly declared, and actively used in generating the final state between Alice and Bob. These results can be used by Eve and as such must be taken care of in the security analysis. As a consequence, we can write the final secure key rate as

$$r \geq p_0 [I(A : B) - \chi(A : E)]. \quad (4)$$

Simulation results.—Our protocol, as detailed above, comprises of two quantum channels: one between Alice and Charlie and another between Bob and Charlie. We assume that the transmittance of both the channels is given by T_A and T_B , respectively, such that, $T_A = 10^{-l \frac{L_{AC}}{10}}$ and $T_B = 10^{-l \frac{L_{BC}}{10}}$, where $l = 0.2$ dB/km is the standard channel loss for telecom wavelength [12, 16] and L_{AC} and L_{BC} are the transmission distances between Alice-Charlie and Bob-Charlie respectively. We assume that Charlie is midway between Alice and Bob such that $L_{AC} = L_{BC} = L/2$ such that the total transmission distance is L . We make this assumption because it has been shown that DV-MDI QKD is much

more efficient when Charlie is midway between Alice and Bob [25]. The secure key rate between Alice and Bob is given by Eq. (4). (See Appendix C 1 for the underlying assumptions made and the evaluation of the secure key rate.)

In Fig. 2, we plot the secure key rate as a function the total transmission distance L . We choose the parameters $\eta_h = 0.55$, $\eta_0 = 0.8$, and $p = \frac{\pi}{2}$ to be as realistic as possible. We see that the total transmission distance can reach upto 300 km with a secure key rate of the order of 10^{-9} bits/pulses for $\alpha = 0.5$ and $l = 0.2$ dB/km. For an ultralow loss fibre [20] with $l = 0.16$ dB/km and $\alpha = 0.5$ we find that it is possible to achieve a total transmission distance of 460 km. However, as we increase α , the key rate is found to decrease drastically. We also find that decreasing the value of α below 0.5 also decreases the key rate as well as the maximum transmission distance leading to an optimal choice of $\alpha \sim 0.5$ (see Appendix C 2).

This optimal value for α is in agreement with the observation that it is also the value of α which is more robust to transmission losses (see Appendix D). The effect of a quantum state passing through a noisy channel can be seen as the system undergoing photon loss. Let us denote the photon loss fraction by R such that $R = 0$ and $R = 1$ correspond to no photon loss and complete photon loss, respectively. In Fig. 3, we show that the entanglement content of an HE state, as given by logarithmic negativity [53], achieves a maximum value for $0 \leq \alpha \leq 1$. For a significantly lossy channel, we find that the optimal value of α approaches $\alpha = 0.5$.

This behaviour of HE states can be qualitatively understood in terms of the interplay between entanglement

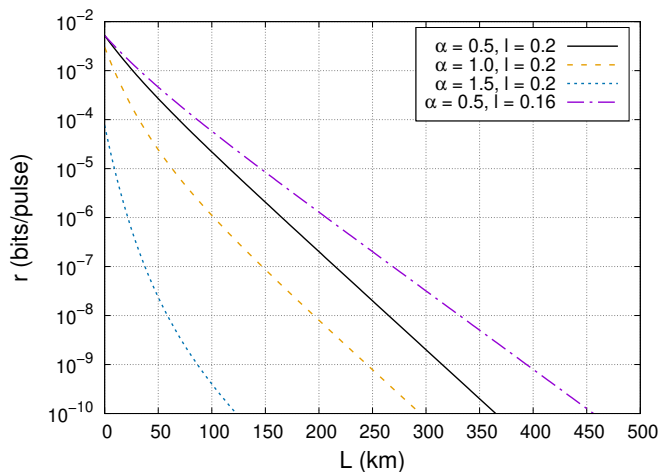


FIG. 2. Secure key rate as a function of total transmission distance L for different values of α and channel loss parameter l (dB/km). We assume detection efficiencies $\eta_h = 0.55$ for the homodyne detectors, $\eta_0 = 0.8$ for the on-off detectors, and $p = \frac{\pi}{2}$.

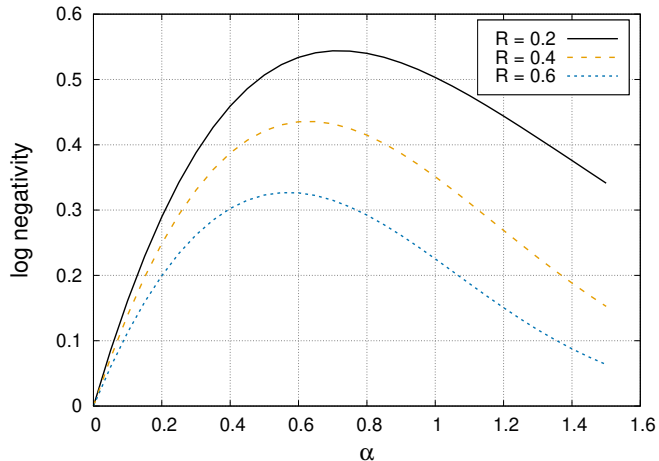


FIG. 3. Logarithmic negativity of the HE state undergoing photon-loss over the CV part as a function of the coherent amplitude α . R ($0 \leq R \leq 1$) stands for the normalized strength of loss.

and the fragility of the initial HE state. Starting from the initial separable state at $\alpha = 0$, the HE state becomes more entangled as α increases. An increase in α also corresponds to an increase in the average number of photons, which can be understood as an increase in the mean energy of the system. However, with an increase in the mean energy, the state becomes more vulnerable to decoherence. This behaviour is similar to what is also shown in Ref. [54] for superposition of coherent states with increasing values of coherent amplitude. As a consequence, with increase in α beyond an optimal value, the HE state becomes extremely fragile under noise leading to a drop in entanglement when the multiphoton

part passes through a noisy quantum channel. See Appendix D for a detailed analysis.

Conclusions.—We have shown that HE states between CV and DV systems provide a robust practical solution to the problem of achieving long-distance high-rate entanglement. Both requirements are fundamental for a number of applications. We have focused on MDI-QKD, as it is both a fundamental application and a multipurpose test bed. In a MDI-QKD setup, our results indicate that HE states bring forth the best of both CV and DV systems, resulting in a secure key rate of $\sim 10^{-9}$ bits/pulse at a distance of 300 km. This, in itself, represents a significant improvement than the best previous results at telecommunication wavelength (a key rate of 10^{-10} bits/pulse at ~ 220 km [12]). All this, without using ultralow-loss fibre (with channel loss $l = 0.16$ dB/km at 1550 nm [20]). With such a fibre, our approach would allow us to achieve $\sim 10^{-10}$ bits/pulse at a distance of 460 km.

The feasibility of the protocol relies in the fact that HE states with small coherent amplitudes ($\alpha < 1$) can be generated in the lab by several non-deterministic techniques [42, 43] and the generation rate is comparable to the rate of entangled photon pairs in parametric down conversion setups. As an example, it is possible to prepare HE states where CV and DV parts correspond to photon number state and coherent state, respectively, with fidelity ≈ 0.75 for $\alpha = 0.5$ [42]. While the rate of generation in the source is comparable to that of parametric down conversion sources, losses during transmission are reduced, so the effective rate at destination increases. The fidelity of the preparation could be a limiting factor. However, this can be mitigated by using other forms of HE states, most notably with the CV and DV modes corresponding to cat states and polarization, respectively, which offer exceptionally good fidelity of preparation as well as rate of generation [55–59].

Our results highlight the significance of HE states as a resource in high-rate remote entanglement generation, which plays a crucial role in enhancing many quantum information processing tasks such as quantum internet [21, 60], quantum digital signature [61, 62], and network steering [63]. We believe that our scheme has the potential to drive a new generation of experimental developments in quantum information technology.

This work is supported by QuantERA grant SECRET, by MCINN/AEI (Project No. PCI2019-111885-2). AC is also supported by MCINN/AEI (Project No. PID2020-113738GB-I00). HJ is supported by National Research Foundation of Korea (NRF) grants funded by the Korean government (Grant Nos. NRF-2020R1A2C1008609, 2023R1A2C1006115 and NRF-2022M3E4A1076099) via the Institute of Applied Physics at Seoul National University, and by the Institute of Information & Communications Technology Planning & Evaluation (IITP) grant funded by the Korea government (MSIT) (IITP-2021-0-01059 and IITP-2023-2020-0-01606).

- [1] B. Hensen, H. Bernien, A. E. Dréau, A. Reiserer, N. Kalb, M. S. Blok, J. Ruitenbergh, R. F. L. Vermeulen, R. N. Schouten, C. Abellán, W. Amaya, V. Pruneri, M. W. Mitchell, M. Markham, D. J. Twitchen, D. Elkouss, S. Wehner, T. H. Taminiau, and R. Hanson, Loophole-free Bell inequality violation using electron spins separated by 1.3 kilometres, *Nature* **526**, 682 (2015).
- [2] W. Rosenfeld, D. Burchardt, R. Garthoff, K. Redeker, N. Ortiegel, M. Rau, and H. Weinfurter, Event-ready Bell test using entangled atoms simultaneously closing detection and locality loopholes, *Phys. Rev. Lett.* **119**, 010402 (2017).
- [3] B. Wittmann, S. Ramelow, F. Steinlechner, N. K. Langford, N. Brunner, H. M. Wiseman, R. Ursin, and A. Zeilinger, Loophole-free Einstein–Podolsky–Rosen experiment via quantum steering, *New J. Phys.* **14**, 053030 (2012).
- [4] X.-S. Ma, T. Herbst, T. Scheidl, D. Wang, S. Kropatschek, W. Naylor, B. Wittmann, A. Mech, J. Kofler, E. Anisimova, V. Makarov, T. Jennewein, R. Ursin, and A. Zeilinger, Quantum teleportation over 143 kilometres using active feed-forward, *Nature* **489**, 269 (2012).
- [5] D. P. Nadlinger, P. Drmota, B. C. Nichol, G. Araneda, D. Main, R. Srinivas, D. M. Lucas, C. J. Ballance, K. Ivanov, E. Y. Z. Tan, P. Sekatski, R. L. Urbanke, R. Renner, N. Sangouard, and J.-D. Bancal, Experimental quantum key distribution certified by Bell’s theorem, *Nature* **607**, 682 (2022).
- [6] W. Zhang, T. van Leent, K. Redeker, R. Garthoff, R. Schwonnek, F. Fertig, S. Eppelt, W. Rosenfeld, V. Scarani, C. C. W. Lim, and H. Weinfurter, A device-independent quantum key distribution system for distant users, *Nature* **607**, 687 (2022).
- [7] W.-Z. Liu, Y.-Z. Zhang, Y.-Z. Zhen, M.-H. Li, Y. Liu, J. Fan, F. Xu, Q. Zhang, and J.-W. Pan, Toward a photonic demonstration of device-independent quantum key distribution, *Phys. Rev. Lett.* **129**, 050502 (2022).
- [8] N. Gisin, S. Pironio, and N. Sangouard, Proposal for implementing device-independent quantum key distribution based on a heralded qubit amplifier, *Phys. Rev. Lett.* **105**, 070501 (2010).
- [9] A. Cabello and F. Sciarrino, Loophole-free bell test based on local precertification of photon’s presence, *Phys. Rev. X* **2**, 021010 (2012).
- [10] E. Meyer-Scott, D. McCloskey, K. Gołos, J. Z. Salvail, K. A. G. Fisher, D. R. Hamel, A. Cabello, K. J. Resch, and T. Jennewein, Certifying the presence of a photonic qubit by splitting it in two, *Phys. Rev. Lett.* **116**, 070501 (2016).
- [11] A. Z. Leger, S. Gambhir, J. Légère, and D. R. Hamel, Amplification of cascaded downconversion by reusing photons with a switchable cavity, *arXiv:2209.11668* (2022).
- [12] H.-K. Lo, M. Curty, and B. Qi, Measurement-device-independent quantum key distribution, *Phys. Rev. Lett.* **108**, 130503 (2012).
- [13] T. Ferreira da Silva, D. Vitoreti, G. B. Xavier, G. C. do Amaral, G. P. Temporão, and J. P. von der Weid, Proof-of-principle demonstration of measurement-device-independent quantum key distribution using polarization qubits, *Phys. Rev. A* **88**, 052303 (2013).
- [14] S. L. Braunstein and S. Pirandola, Side-channel-free quantum key distribution, *Phys. Rev. Lett.* **108**, 130502 (2012).
- [15] C. Ottaviani, G. Spedalieri, S. L. Braunstein, and S. Pirandola, Continuous-variable quantum cryptography with an untrusted relay: Detailed security analysis of the symmetric configuration, *Phys. Rev. A* **91**, 022320 (2015).
- [16] S. Pirandola, C. Ottaviani, G. Spedalieri, C. Weedbrook, S. L. Braunstein, S. Lloyd, T. Gehring, C. S. Jacobsen, and U. L. Andersen, High-rate measurement-device-independent quantum cryptography, *Nat. Photonics* **9**, 397 (2015).
- [17] C. Kumar, J. Singh, S. Bose, and Arvind, Coherence-assisted non-Gaussian measurement-device-independent quantum key distribution, *Phys. Rev. A* **100**, 052329 (2019).
- [18] J. Singh and S. Bose, Non-Gaussian operations in measurement-device-independent quantum key distribution, *Phys. Rev. A* **104**, 052605 (2021).
- [19] Y.-L. Tang, H.-L. Yin, S.-J. Chen, Y. Liu, W.-J. Zhang, X. Jiang, L. Zhang, J. Wang, L.-X. You, J.-Y. Guan, D.-X. Yang, Z. Wang, H. Liang, Z. Zhang, N. Zhou, X. Ma, T.-Y. Chen, Q. Zhang, and J.-W. Pan, Measurement-device-independent quantum key distribution over 200 km, *Phys. Rev. Lett.* **113**, 190501 (2014).
- [20] Y.-L. Tang, H.-L. Yin, S.-J. Chen, Y. Liu, W.-J. Zhang, X. Jiang, L. Zhang, J. Wang, L.-X. You, J.-Y. Guan, D.-X. Yang, Z. Wang, H. Liang, Z. Zhang, N. Zhou, X. Ma, T.-Y. Chen, Q. Zhang, and J.-W. Pan, Field test of measurement-device-independent quantum key distribution, *IEEE J. Sel. Top. Quantum Electron.* **21**, 116 (2015).
- [21] Y.-L. Tang, H.-L. Yin, Q. Zhao, H. Liu, X.-X. Sun, M.-Q. Huang, W.-J. Zhang, S.-J. Chen, L. Zhang, L.-X. You, Z. Wang, Y. Liu, C.-Y. Lu, X. Jiang, X. Ma, Q. Zhang, T.-Y. Chen, and J.-W. Pan, Measurement-device-independent quantum key distribution over untrusted metropolitan network, *Phys. Rev. X* **6**, 011024 (2016).
- [22] B. Fröhlich, J. F. Dynes, M. Lucamarini, A. W. Sharpe, Z. Yuan, and A. J. Shields, A quantum access network, *Nature* **501**, 69 (2013).
- [23] H.-L. Yin, T.-Y. Chen, Z.-W. Yu, H. Liu, L.-X. You, Y.-H. Zhou, S.-J. Chen, Y. Mao, M.-Q. Huang, W.-J. Zhang, H. Chen, M. J. Li, D. Nolan, F. Zhou, X. Jiang, Z. Wang, Q. Zhang, X.-B. Wang, and J.-W. Pan, Measurement-device-independent quantum key distribution over a 404 km optical fiber, *Phys. Rev. Lett.* **117**, 190501 (2016).
- [24] E. Diamanti, H.-K. Lo, B. Qi, and Z. Yuan, Practical challenges in quantum key distribution, *npj Quantum Inf.* **2**, 16025 (2016).
- [25] F. Xu, M. Curty, B. Qi, L. Qian, and H.-K. Lo, Discrete and continuous variables for measurement-device-independent quantum cryptography, *Nat. Photonics* **9**, 772 (2015).
- [26] H. Jeong, Using weak nonlinearity under decoherence for macroscopic entanglement generation and quantum computation, *Phys. Rev. A* **72**, 034305 (2005).
- [27] Y. Li, H. Jing, and M.-S. Zhan, Optical generation of a

- hybrid entangled state via an entangling single-photon-added coherent state, *J. Phys. B: At. Mol. Opt. Phys.* **39**, 2107 (2006).
- [28] J.-Q. Liao, Y. Guo, H.-S. Zeng, and L.-M. Kuang, Preparation of hybrid entangled states and entangled coherent states for a single trapped ion in a cavity, *J. Phys. B: At. Mol. Opt. Phys.* **39**, 4709 (2006).
- [29] B. He, Q. Lin, and C. Simon, Cross-Kerr nonlinearity between continuous-mode coherent states and single photons, *Phys. Rev. A* **83**, 053826 (2011).
- [30] M. Hosseini, S. Rebic, B. M. Sparkes, J. Twamley, B. C. Buchler, and P. K. Lam, Memory-enhanced noiseless cross-phase modulation, *Light: Sci. Appl.* **1**, e40 (2012).
- [31] Z.-B. Chen, G. Hou, and Y.-D. Zhang, Quantum nonlocality and applications in quantum-information processing of hybrid entangled states, *Phys. Rev. A* **65**, 032317 (2002).
- [32] K. Park, S.-W. Lee, and H. Jeong, Quantum teleportation between particlelike and fieldlike qubits using hybrid entanglement under decoherence effects, *Phys. Rev. A* **86**, 062301 (2012).
- [33] H. Kwon and H. Jeong, Violation of the Bell–Clauser–Horne–Shimony–Holt inequality using imperfect photodetectors with optical hybrid states, *Phys. Rev. A* **88**, 052127 (2013).
- [34] S.-W. Lee and H. Jeong, Near-deterministic quantum teleportation and resource-efficient quantum computation using linear optics and hybrid qubits, *Phys. Rev. A* **87**, 022326 (2013).
- [35] U. L. Andersen, J. S. Neergaard-Nielsen, P. van Loock, and A. Furusawa, Hybrid discrete and continuous-variable quantum information, *Nat. Phys.* **11**, 713 (2015).
- [36] S. Omkar, Y. S. Teo, and H. Jeong, Resource-efficient topological fault-tolerant quantum computation with hybrid entanglement of light, *Phys. Rev. Lett.* **125**, 060501 (2020).
- [37] S. Omkar, Y. S. Teo, S.-W. Lee, and H. Jeong, Highly photon-loss-tolerant quantum computing using hybrid qubits, *Phys. Rev. A* **103**, 032602 (2021).
- [38] S. Bose and H. Jeong, Quantum teleportation of hybrid qubits and single-photon qubits using Gaussian resources, *Phys. Rev. A* **105**, 032434 (2022).
- [39] M. He and R. Malaney, Teleportation of hybrid entangled states with continuous-variable entanglement, *Sci. Rep.* **12**, 17169 (2022).
- [40] Y.-B. Sheng, L. Zhou, and G.-L. Long, Hybrid entanglement purification for quantum repeaters, *Phys. Rev. A* **88**, 022302 (2013).
- [41] Y. Lim, J. Joo, T. P. Spiller, and H. Jeong, Loss-resilient photonic entanglement swapping using optical hybrid states, *Phys. Rev. A* **94**, 062337 (2016).
- [42] H. Jeong, A. Zavatta, M. Kang, S.-W. Lee, L. S. Costanzo, S. Grandi, T. C. Ralph, and M. Bellini, Generation of hybrid entanglement of light, *Nat. Photonics* **8**, 564 (2014).
- [43] O. Morin, K. Huang, J. Liu, L. H. Jeannic, C. Fabre, and J. Laurat, Remote creation of hybrid entanglement between particle-like and wave-like optical qubits, *Nat. Photonics* **8**, 570 (2014).
- [44] A. E. Ulanov, D. Sychev, A. A. Pushkina, I. A. Fedorov, and A. I. Lvovsky, Quantum teleportation between discrete and continuous encodings of an optical qubit, *Phys. Rev. Lett.* **118**, 160501 (2017).
- [45] D. V. Sychev, A. E. Ulanov, E. S. Tiunov, A. A. Pushkina, A. Kuzhamuratov, V. Novikov, and A. I. Lvovsky, Entanglement and teleportation between polarization and wave-like encodings of an optical qubit, *Nature Communications* **9**, 3672 (2018).
- [46] T. Darras, B. E. Asenbeck, G. Guccione, A. Cavaillès, H. Le Jeannic, and J. Laurat, A quantum-bit encoding converter, *Nat. Photonics* **17**, 165 (2023).
- [47] B. Qi, P. Lougovski, R. Pooser, W. Grice, and M. Bobrek, Generating the local oscillator “locally” in continuous-variable quantum key distribution based on coherent detection, *Phys. Rev. X* **5**, 041009 (2015).
- [48] P. Jouguet, S. Kunz-Jacques, A. Leverrier, P. Grangier, and E. Diamanti, Experimental demonstration of long-distance continuous-variable quantum key distribution, *Nat. Photonics* **7**, 378 (2013).
- [49] M. Zou, Y. Mao, and T.-Y. Chen, Rigorous calibration of homodyne detection efficiency for continuous-variable quantum key distribution, *Opt. Express* **30**, 22788 (2022).
- [50] G. Zhang, J. Y. Haw, H. Cai, F. Xu, S. M. Assad, J. F. Fitzsimons, X. Zhou, Y. Zhang, S. Yu, J. Wu, W. Ser, L. C. Kwek, and A. Q. Liu, An integrated silicon photonic chip platform for continuous-variable quantum key distribution, *Nat. Photonics* **13**, 839 (2019).
- [51] Y. Zhang, Z. Chen, S. Pirandola, X. Wang, C. Zhou, B. Chu, Y. Zhao, B. Xu, S. Yu, and H. Guo, Long-distance continuous-variable quantum key distribution over 202.81 km of fiber, *Phys. Rev. Lett.* **125**, 010502 (2020).
- [52] While a photon-number-resolving-detector (PNRD) measures the number of photons detected, an on-off detector only indicates whether a photon is detected or not. As a consequence, an on-off detector is much less demanding than a PNRD. Recent advances in technology has led to development of single-photon detectors with efficiencies as high as 0.84–0.91 [64–66] with the use of high-contrast-grating in nanophotonics settings. This, in turn, implies that the efficiency of an on-off detector can be safely approximated upto 0.80 (if not more).
- [53] M. B. Plenio, Logarithmic negativity: A full entanglement monotone that is not convex, *Phys. Rev. Lett.* **95**, 090503 (2005).
- [54] C.-W. Lee and H. Jeong, Quantification of macroscopic quantum superpositions within phase space, *Phys. Rev. Lett.* **106**, 220401 (2011).
- [55] H. Kwon and H. Jeong, Generation of hybrid entanglement between a single-photon polarization qubit and a coherent state, *Phys. Rev. A* **91**, 012340 (2015).
- [56] S. Li, H. Yan, Y. He, and H. Wang, Experimentally feasible generation protocol for polarized hybrid entanglement, *Phys. Rev. A* **98**, 022334 (2018).
- [57] S. A. Podoshvedov and N. B. An, Designs of interactions between discrete and continuous-variable states for generation of hybrid entanglement, *Quant. Inf. Process.* **18**, 68 (2019).
- [58] K. Huang, H. L. Jeannic, O. Morin, T. Darras, G. Guccione, A. Cavaillès, and J. Laurat, Engineering optical hybrid entanglement between discrete- and continuous-variable states, *New J. Phys.* **21**, 083033 (2019).
- [59] J. Wen, I. Novikova, C. Qian, C. Zhang, and S. Du, Hybrid entanglement between optical discrete polarizations and continuous quadrature variables, *Photonics* **8**, 552 (2021).
- [60] S. Wehner, D. Elkouss, and R. Hanson, Quantum inter-

- net: A vision for the road ahead, *Science* **362**, eaam9288 (2018).
- [61] H.-L. Yin, Y. Fu, H. Liu, Q.-J. Tang, J. Wang, L.-X. You, W.-J. Zhang, S.-J. Chen, Z. Wang, Q. Zhang, T.-Y. Chen, Z.-B. Chen, and J.-W. Pan, Experimental quantum digital signature over 102 km, *Phys. Rev. A* **95**, 032334 (2017).
- [62] W. Zhao, R. Shi, J. Shi, P. Huang, Y. Guo, and D. Huang, Multibit quantum digital signature with continuous variables using basis encoding over insecure channels, *Phys. Rev. A* **103**, 012410 (2021).
- [63] B. D. M. Jones, I. Šupić, R. Uola, N. Brunner, and P. Skrzypczyk, Network quantum steering, *Phys. Rev. Lett.* **127**, 170405 (2021).
- [64] W. Pernice, C. Schuck, O. Minaeva, M. Li, G. Goltsman, A. Sergienko, and H. Tang, High-speed and high-efficiency travelling wave single-photon detectors embedded in nanophotonic circuits, *Nat. Commun.* **3**, 1325 (2012).
- [65] C. Wei, W. Wang, D. Liu, M. Gu, and X. Wu, High-efficiency and large light-receiving area superconducting nanowire single-photon detector integrated with high-contrast grating, *Photon. Res.* **9**, 2253 (2021).
- [66] S. Miki, S. Miyajima, F. China, M. Yabuno, and H. Terai, Photon detection at 1 ns time intervals using 16-element SNSPD array with SFQ multiplexer, *Opt. Lett.* **46**, 6015 (2021).
- [67] S. M. Barnett, D. T. Pegg, and J. Jeffers, Equivalence of a lossless beam splitter and a nondegenerate parametric amplifier in conditional measurements, *Opt. Commun.* **172**, 55 (1999).
- [68] K. Życzkowski, P. Horodecki, A. Sanpera, and M. Lewenstein, Volume of the set of separable states, *Phys. Rev. A* **58**, 883 (1998).

APPENDIX

Appendix A: Generation of the hybrid entangled state

In this section we outline a process, using a setup in line with Ref. [42], that can be used to experimentally generate a hybrid entangled (HE) state of the form

$$|\psi\rangle_{ab} = \frac{1}{\sqrt{2}} (|0\rangle_a |\alpha\rangle_b + |1\rangle_a |-\alpha\rangle_b) \quad (\text{A1})$$

between modes a and b , where $|0\rangle$ and $|1\rangle$ correspond to photon number states, and $|\alpha\rangle$ is the coherent state with coherent amplitude α .

$|n\rangle$ and $|\alpha\rangle$ correspond to, respectively, the energy eigenstate and coherent state of a quantized electromagnetic field, where n is the number of photons in the state. It is possible to realize the energy eigenstates as a single-photon qubit by only considering the photon number states corresponding to $|0\rangle$ and $|1\rangle$. This is our discrete variable (DV) system and the multiphoton coherent state is our continuous variable (CV) system. The key idea of HE state generation hinges on conditional photon addition and erasing the path information of photon addition. There are several ways of achieving photon addition. This includes a model which uses single photon sources and beam splitters (BS) and another model which uses a parametric-down-converter (PDC) with a weak pump. Since the BS setup and the PDC are equivalent [67], here we use the BS model for photon addition. The following is a step-by-step description of the generation of the HE state in Fig. 1(b) of the main text.

Step 1: A vacuum state $|0\rangle$ in mode a is mixed with a single-photon state $|1\rangle$ in mode c using a BS (BS_1) with transmittivity T . Similarly, a coherent state $|\alpha\rangle$ in mode c is mixed with another single-photon state in mode d using another BS (BS_2) with transmittivity T . The output states from each of these two BSs are

$$|\psi\rangle_{ac}^{\text{BS}_1} = \sqrt{1-T} |1\rangle_a |0\rangle_c + \sqrt{T} |0\rangle_a |1\rangle_c \quad \text{and} \quad |\psi\rangle_{bd}^{\text{BS}_2} = \sqrt{1-T} \hat{b}^\dagger |\alpha\rangle_b |0\rangle_d + \sqrt{T} |\alpha\rangle_b |1\rangle_d, \quad (\text{A2})$$

where \hat{b}^\dagger is the creation operator acting on mode b and $|\psi\rangle_{ac}^{\text{BS}_1}$ is the output state from BS_1 , while $|\psi\rangle_{bd}^{\text{BS}_2}$ is the output state from BS_2 . The BS transmittivity T can be fine-tuned according to experimental requirements to yield maximum probability for photon addition. Therefore, the 4-mode state at the output of BS_1 and BS_2 is

$$\begin{aligned} |\psi\rangle_{ab,cd}^{\text{BS}_1, \text{BS}_2} = & \sqrt{T(1-T)} \left(|1\rangle_a |\alpha\rangle_b \otimes |0\rangle_c |1\rangle_d + |0\rangle_a \hat{b}^\dagger |\alpha\rangle_b \otimes |1\rangle_c |0\rangle_d \right) \\ & + (1-T) |1\rangle_a \hat{b}^\dagger |\alpha\rangle_b \otimes |0\rangle_c |0\rangle_d + T |0\rangle_a |\alpha\rangle_b \otimes |1\rangle_c |1\rangle_d. \end{aligned} \quad (\text{A3})$$

Step 2: The outgoing single-photon modes (shown by gray dashed-lines in Fig. 1(b) of the main text) from both BS_1 and BS_2 are mixed with each other using another BS (BS_3) with transmittivity τ . This leads to a 4-mode state at the output of BS_3 which can be written as

$$\begin{aligned} |\psi\rangle_{ab,cd}^{\text{BS}_3} = & \sqrt{T(1-T)} \left[|1\rangle_a |\alpha\rangle_b \otimes \left(-\sqrt{1-\tau} |0\rangle_c |1\rangle_d + \sqrt{\tau} |1\rangle_c |0\rangle_d \right) + |0\rangle_a \hat{b}^\dagger |\alpha\rangle_b \otimes \left(\sqrt{1-\tau} |1\rangle_c |0\rangle_d + \sqrt{\tau} |0\rangle_c |1\rangle_d \right) \right] \\ & + (1-T) |1\rangle_a \hat{b}^\dagger |\alpha\rangle_b \otimes |0\rangle_c |0\rangle_d + T |0\rangle_a |\alpha\rangle_b \otimes \left(\sqrt{1-\tau} |2\rangle_c |0\rangle_d + \sqrt{\tau} |0\rangle_c |2\rangle_d \right). \end{aligned} \quad (\text{A4})$$

Step 3: We now detect the output modes of BS₃ via single-photon detectors D₁ and D₂. Since the total photon number at the output of BS₃ is 1, it indicates that both D₁ and D₂ cannot click simultaneously. We post-select the state when only the detector D₁ clicks and discard the runs whenever the detector D₂ clicks. After post-selection, the state between modes a and b is

$$|\psi\rangle_{ab}^{\text{D}_1} = \langle 1|_c \langle 0|_d |\psi\rangle_{ab,cd}^{\text{BS}_3} = \sqrt{T(1-T)} \left(\sqrt{\tau} |1\rangle_a |\alpha\rangle_b + \sqrt{1-\tau} |0\rangle_a \hat{b}^\dagger |\alpha\rangle_b \right). \quad (\text{A5})$$

We can now use the fact that n -photon-added coherent state is a good approximation to another coherent state with amplified amplitude, i.e., $\frac{\hat{b}^{\dagger n}}{\sqrt{N}} |\alpha\rangle \approx |g\alpha\rangle$ [42], where N is the corresponding normalization constant and $g \geq 1$ is the amplification factor. This leads to the result $\hat{b}^\dagger |\alpha\rangle_b \approx \frac{1}{\sqrt{1-\alpha^2}} |g\alpha\rangle_b$, where g is properly chosen. Then, by setting $\tau = \frac{1+\alpha^2}{2+\alpha^2}$ and using the approximation we get,

$$|\psi\rangle_{ab}^{\text{D}_1} \approx \sqrt{\frac{T(1-T)}{2+\alpha^2}} \left(|1\rangle_a |\alpha\rangle_b + |0\rangle_a |g\alpha\rangle_b \right). \quad (\text{A6})$$

Step 4: Next, we displace the mode b by performing a displacement operator on this mode given by $D_b \left(-\frac{\alpha+g\alpha}{2} \right) = \exp \left[-\frac{\alpha+g\alpha}{2} (\hat{b}^\dagger - \hat{b}) \right]$, where \hat{b} is the annihilation operator. This leads to the final normalized HE state

$$|\psi\rangle_{ab} = \frac{1}{\sqrt{2}} \left(|0\rangle_a |\alpha_f\rangle_b + |1\rangle_a |-\alpha_f\rangle_b \right), \quad (\text{A7})$$

where $\alpha_f = \frac{(g-1)\alpha}{2}$.

Appendix B: States after every step of the protocol

In this section we calculate the the state obtained after performing the entanglement swapping operation by Charlie. We also calculate the states obtained after every step of the protocol starting from the initial resource of HE states. The steps of the protocol are detailed in the main manuscript.

1. Initial states and channel transmission

We denote the two hybrid entangled states with Alice and Bob as

$$|\psi\rangle_{a_1 a_2} = \frac{1}{\sqrt{2}} \left(|0\rangle_{a_1} |\alpha\rangle_{a_2} + |1\rangle_{a_1} |-\alpha\rangle_{a_2} \right) \quad \text{and} \quad |\psi\rangle_{b_1 b_2} = \frac{1}{\sqrt{2}} \left(|0\rangle_{b_1} |\alpha\rangle_{b_2} + |1\rangle_{b_1} |-\alpha\rangle_{b_2} \right), \quad (\text{B1})$$

respectively. The initial 4-mode resource state can be written as

$$\begin{aligned} |\psi\rangle_{\substack{a_1 a_2 \\ b_1 b_2}} &= |\psi\rangle_{a_1 a_2} |\psi\rangle_{b_1 b_2} \\ &= \frac{1}{2} \left(|00\rangle_{a_1 b_1} |\alpha\rangle_{a_2} |\alpha\rangle_{b_2} + |11\rangle_{a_1 b_1} |-\alpha\rangle_{a_2} |-\alpha\rangle_{b_2} + |01\rangle_{a_1 b_1} |\alpha\rangle_{a_2} |-\alpha\rangle_{b_2} + |10\rangle_{a_1 b_1} |-\alpha\rangle_{a_2} |\alpha\rangle_{b_2} \right), \end{aligned} \quad (\text{B2})$$

where $|ij\rangle_{a_1 b_1} = |i\rangle_{a_1} |j\rangle_{b_1} \forall i, j \in \{0, 1\}$.

Alice and Bob both send their multiphoton part (modes a_2 and b_2) to a third distant party Charlie for mixing and subsequent measurements through a noisy/lossy channel with transmittivity T . Such channels could be modelled in terms of an effective beam splitter (BS) with transmittivity T , where the input state is fed at one of the inputs of the BS while the other input is initialised as a vacuum state. The action of a BS with transmittivity T on the input modes is given by a unitary U_T^{ab} implementing the following transformation:

$$\begin{pmatrix} \hat{a} \\ \hat{b} \end{pmatrix} \rightarrow \begin{pmatrix} \hat{a}' \\ \hat{b}' \end{pmatrix} = \begin{pmatrix} \sqrt{T} & \sqrt{1-T} \\ -\sqrt{1-T} & \sqrt{T} \end{pmatrix} \begin{pmatrix} \hat{a} \\ \hat{b} \end{pmatrix}. \quad (\text{B3})$$

$T = \frac{1}{2}$ corresponds to a balanced (50 : 50) BS. As a consequence, the action of the channel on a coherent state ($|\alpha\rangle$) in mode a is described as $U_T^{ab} |\alpha\rangle_a \otimes |0\rangle_b \rightarrow |\alpha\rangle_{a'} \otimes |0\rangle_{b'} = \left| \sqrt{T}\alpha \right\rangle_a \otimes \left| \sqrt{1-T}\alpha \right\rangle_b$, where U_T^{ab} is the corresponding BS unitary operation. Subsequently, the resultant state is obtained by tracing over the ancillary mode b .

Similarly, the noisy transmission of modes a_2 and b_2 could be described by using two BSs with transmittivity T , each one in the paths of modes a_2 and b_2 with ancillary modes given by f_a and f_b , respectively. The resultant noisy/lossy state is obtained by tracing over the ancillary modes (f_a and f_b). Therefore, the total input state to Charlie before mixing is

$$\begin{aligned} |\psi\rangle_{a_1, b_1; a_2', b_2'} &= U_T^{(a_2, f_a)} \otimes U_T^{(b_2, f_b)} |\psi\rangle_{a_1 a_2} \otimes |0\rangle_{f_a} |0\rangle_{f_b} \\ &= \frac{1}{2} \left(|00\rangle_{a_1 b_1} \left| \sqrt{1-T}\alpha \right\rangle_{f_a} \left| \sqrt{1-T}\alpha \right\rangle_{f_b} \left| \sqrt{T}\alpha \right\rangle_{a_2} \left| \sqrt{T}\alpha \right\rangle_{b_2} + |11\rangle_{a_1 b_1} \left| -\sqrt{1-T}\alpha \right\rangle_{f_a} \left| -\sqrt{1-T}\alpha \right\rangle_{f_b} \left| -\sqrt{T}\alpha \right\rangle_{a_2} \left| -\sqrt{T}\alpha \right\rangle_{b_2} \right. \\ &\quad \left. + |01\rangle_{a_1 b_1} \left| \sqrt{1-T}\alpha \right\rangle_{f_a} \left| -\sqrt{1-T}\alpha \right\rangle_{f_b} \left| \sqrt{T}\alpha \right\rangle_{a_2} \left| -\sqrt{T}\alpha \right\rangle_{b_2} + |10\rangle_{a_1 b_1} \left| -\sqrt{1-T}\alpha \right\rangle_{f_a} \left| \sqrt{1-T}\alpha \right\rangle_{f_b} \left| -\sqrt{T}\alpha \right\rangle_{a_2} \left| \sqrt{T}\alpha \right\rangle_{b_2} \right), \end{aligned} \quad (\text{B4})$$

$$+ |01\rangle_{a_1 b_1} \left| \sqrt{1-T}\alpha \right\rangle_{f_a} \left| -\sqrt{1-T}\alpha \right\rangle_{f_b} \left| \sqrt{T}\alpha \right\rangle_{a_2} \left| -\sqrt{T}\alpha \right\rangle_{b_2} + |10\rangle_{a_1 b_1} \left| -\sqrt{1-T}\alpha \right\rangle_{f_a} \left| \sqrt{1-T}\alpha \right\rangle_{f_b} \left| -\sqrt{T}\alpha \right\rangle_{a_2} \left| \sqrt{T}\alpha \right\rangle_{b_2} \right), \quad (\text{B5})$$

where $U_T^{(a_2, f_a)}$ and $U_T^{(b_2, f_b)}$ are the BS unitary operations corresponding to the respective channels with transmittivity T . Charlie now mixes the incoming multiphoton modes (a_2 and b_2) through a balanced BS (BS₁) leading to the four mode entangled state

$$\begin{aligned} |\psi\rangle_{a_1, b_1; a_2'', b_2''}^{\text{BS}_1} &= U_{\text{BS}_1}^{(a_2, b_2)} |\psi\rangle_{a_1, b_1; a_2', b_2'} \\ &= \frac{1}{2} \left(|00\rangle_{a_1 b_1} \left| \sqrt{1-T}\alpha \right\rangle_{f_a} \left| \sqrt{1-T}\alpha \right\rangle_{f_b} |0\rangle_{b_2} \left| \sqrt{2T}\alpha \right\rangle_{a_2} + |11\rangle_{a_1 b_1} \left| -\sqrt{1-T}\alpha \right\rangle_{f_a} \left| -\sqrt{1-T}\alpha \right\rangle_{f_b} |0\rangle_{b_2'} \left| -\sqrt{2T}\alpha \right\rangle_{a_2} \right. \\ &\quad \left. + |01\rangle_{a_1 b_1} \left| \sqrt{1-T}\alpha \right\rangle_{f_a} \left| -\sqrt{1-T}\alpha \right\rangle_{f_b} \left| \sqrt{2T}\alpha \right\rangle_{b_2} |0\rangle_{a_2} + |10\rangle_{a_1 b_1} \left| -\sqrt{1-T}\alpha \right\rangle_{f_a} \left| \sqrt{1-T}\alpha \right\rangle_{f_b} \left| -\sqrt{2T}\alpha \right\rangle_{b_2} |0\rangle_{a_2} \right). \end{aligned} \quad (\text{B6})$$

It can be seen from Eq. (B6) that, in the total 4-mode entangled state after mixing by Charlie, the vacuum state contribution in mode a_2 appears with probability 1/2. Our primary aim is to postselect the state (B6) in $|0\rangle_{a_2}$.

2. State after the on-off measurement

The additional coherent state sent by Bob to Charlie ($|\sqrt{2}\alpha\rangle$) becomes $|\sqrt{2T}\alpha\rangle$ as a result of transmission through lossy channel. As is described in [42], for this purpose Charlie first mixes the outgoing a_2 mode with this additional state ($|\sqrt{2T}\alpha\rangle$) in mode c through the second balanced beam splitter (BS₂). Consequently, the state after the mixing at BS₂ is given by

$$\begin{aligned} |\psi\rangle_{a_1, b_1; b_2''}^{\text{BS}_2} &= U_{\text{BS}_1}^{(a_2, c)} |\psi\rangle_{a_1, b_1; a_2'', b_2''}^{\text{BS}_1} \otimes |\sqrt{2T}\alpha\rangle_c \\ &= \frac{1}{2} \left(|00\rangle_{a_1 b_1} \left| \sqrt{1-T}\alpha \right\rangle_{f_a} \left| \sqrt{1-T}\alpha \right\rangle_{f_b} |0\rangle_{b_2} \left| 2\sqrt{T}\alpha \right\rangle_{a_2} |0\rangle_c \right. \\ &\quad + |11\rangle_{a_1 b_1} \left| -\sqrt{1-T}\alpha \right\rangle_{f_a} \left| -\sqrt{1-T}\alpha \right\rangle_{f_b} |0\rangle_{b_2} |0\rangle_{a_2} \left| -2\sqrt{T}\alpha \right\rangle_c \\ &\quad + |01\rangle_{a_1 b_1} \left| \sqrt{1-T}\alpha \right\rangle_{f_a} \left| -\sqrt{1-T}\alpha \right\rangle_{f_b} \left| \sqrt{2T}\alpha \right\rangle_{b_2} \left| \sqrt{T}\alpha \right\rangle_{a_2} \left| -\sqrt{T}\alpha \right\rangle_c \\ &\quad \left. + |10\rangle_{a_1 b_1} \left| -\sqrt{1-T}\alpha \right\rangle_{f_a} \left| \sqrt{1-T}\alpha \right\rangle_{f_b} \left| -\sqrt{2T}\alpha \right\rangle_{b_2} \left| \sqrt{T}\alpha \right\rangle_{a_2} \left| -\sqrt{T}\alpha \right\rangle_c \right). \end{aligned} \quad (\text{B7})$$

As it can be seen from Eq. (B7), if both the detectors at the output of BS₂ click then the contribution can arise only from the respective part in (B7), i.e., from the part containing $|0\rangle_{a_2}$. Experimentally, this could be achieved unambiguously by performing the operation $\Pi_0 = (\mathbf{I} - |0\rangle\langle 0|) \otimes (\mathbf{I} - |0\rangle\langle 0|)$ on (B7) using two *on-off* detectors at both the output ports of BS₂.

However, here we consider *non-ideal* detectors with efficiency η_o ($0 \leq \eta_o \leq 1$). Similar to the case of transmission channels, this could be analysed by considering two additional BS with transmittivity η_o and two ancillary modes g_a and g_c for modes a_2 and c , respectively. Therefore, before the *on-off* detectors, the total state is given by

$$\begin{aligned}
|\psi\rangle_{\substack{a_1, b_1; b_2'' \\ f_a', f_b', g_a', g_c' \\ a_2, c}}^{tot} &= U_{\eta_o}^{(a_2, g_a)} \otimes U_{\eta_o}^{(c, g_c)} |\psi\rangle_{\substack{a_1, b_1; b_2'' \\ f_a', f_b' \\ a_2, c}}^{\text{BS}_2} \otimes |0\rangle_{g_a} |0\rangle_{g_c} \\
&= \frac{1}{2} \left[|00\rangle_{a_1 b_1} |0\rangle_{b_2''} \left| \sqrt{1-T}\alpha \right\rangle_{f_a} \left| \sqrt{1-T}\alpha \right\rangle_{f_b} \left| 2\sqrt{T(1-\eta_o)}\alpha \right\rangle_{g_a} |0\rangle_{g_c} \left| 2\sqrt{T\eta_o}\alpha \right\rangle_{a_2} |0\rangle_c \right. \\
&\quad + |11\rangle_{a_1 b_1} |0\rangle_{b_2} \left| -\sqrt{1-T}\alpha \right\rangle_{f_a} \left| -\sqrt{1-T}\alpha \right\rangle_{f_b} |0\rangle_{g_a} \left| -2\sqrt{T(1-\eta_o)}\alpha \right\rangle_{g_c} |0\rangle_{a_2} \left| -2\sqrt{T\eta_o}\alpha \right\rangle_c \\
&\quad + \left(|01\rangle_{a_1 b_1} \left| \sqrt{2T}\alpha \right\rangle_{b_2} \left| \sqrt{1-T}\alpha \right\rangle_{f_a} \left| -\sqrt{1-T}\alpha \right\rangle_{f_b} + |10\rangle_{a_1 b_1} \left| -\sqrt{2T}\alpha \right\rangle_{b_2} \left| -\sqrt{1-T}\alpha \right\rangle_{f_a} \left| \sqrt{1-T}\alpha \right\rangle_{f_b} \right) \\
&\quad \left. \left| \sqrt{T(1-\eta_o)}\alpha \right\rangle_{g_a} \left| -\sqrt{T(1-\eta_o)}\alpha \right\rangle_{g_c} \left| \sqrt{T\eta_o}\alpha \right\rangle_{a_2} \left| -\sqrt{T\eta_o}\alpha \right\rangle_c \right] \\
&= \frac{1}{2} \left[|00\rangle_{a_1 b_1} |0\rangle_{b_2} \left| \sqrt{T'}\alpha \right\rangle_{f_a} \left| \sqrt{T'}\alpha \right\rangle_{f_b} \left| 2\sqrt{T\eta_o'}\alpha \right\rangle_{g_a} |0\rangle_{g_c} \left| 2\sqrt{T\eta_o}\alpha \right\rangle_{a_2} |0\rangle_c \right. \\
&\quad + |11\rangle_{a_1 b_1} |0\rangle_{b_2} \left| -\sqrt{T'}\alpha \right\rangle_{f_a} \left| -\sqrt{T'}\alpha \right\rangle_{f_b} |0\rangle_{g_a} \left| -2\sqrt{T\eta_o'}\alpha \right\rangle_{g_c} |0\rangle_{a_2} \left| -2\sqrt{T\eta_o}\alpha \right\rangle_c \\
&\quad + \left(|01\rangle_{a_1 b_1} \left| \sqrt{2T}\alpha \right\rangle_{b_2} \left| \sqrt{T'}\alpha \right\rangle_{f_a} \left| -\sqrt{T'}\alpha \right\rangle_{f_b} + |10\rangle_{a_1 b_1} \left| -\sqrt{2T}\alpha \right\rangle_{b_2} \left| -\sqrt{T'}\alpha \right\rangle_{f_a} \left| \sqrt{T'}\alpha \right\rangle_{f_b} \right) \\
&\quad \left. \left| \sqrt{T\eta_o'}\alpha \right\rangle_{g_a} \left| -\sqrt{T\eta_o'}\alpha \right\rangle_{g_c} \left| \sqrt{T\eta_o}\alpha \right\rangle_{a_2} \left| -\sqrt{T\eta_o}\alpha \right\rangle_c \right], \tag{B8}
\end{aligned}$$

where $T' = 1 - T$ and $\eta_o' = 1 - \eta_o$.

Charlie is now supposed to make the measurement of $\Pi_0^{a_2, c} = (\mathbf{1} - |0\rangle\langle 0|)_{a_2} \otimes (\mathbf{1} - |0\rangle\langle 0|)_c$ on the state in Eq. (B8). After the measurement of these operators (Π_0) the total state collapses to $\rho_{a_1, b_1; b_2}^0 = \text{tr}_{\substack{f_a, f_b \\ g_a, g_c \\ a_2, c}}^{f_a, f_b} (|\psi_0\rangle\langle\psi_0|) / N_0$, where

$|\psi_0\rangle = \Pi_0^{a_2, c} |\psi\rangle_{\substack{a_1, b_1; b_2'' \\ f_a', f_b', g_a', g_c' \\ a_2, c}}^{tot}$ and the normalization constants are $N_0 = \text{tr}_{\substack{f_a, f_b, g_a, g_c \\ a_2, c}}^{f_a, f_b, g_a, g_c} (|\psi_0\rangle\langle\psi_0|)$. It must be noted that

the state $\rho_{a_1, b_1; b_2}^0$ is obtained with probability $P_0 = \text{tr}_{b_2} (\rho_{a_1, b_1; b_2}^0)$.

Let us look at the result first

$$\begin{aligned}
\Pi_0^{a_2, c} |\alpha\rangle_{a_2} |\beta\rangle_c &= \left(\mathbf{1}_{a_2} \otimes \mathbf{1}_c - |0\rangle_{a_2} \langle 0| \otimes \mathbf{1}_c - \mathbf{1}_{a_2} \otimes |0\rangle_c \langle 0| + |0\rangle_{a_2} \langle 0| \otimes |0\rangle_c \langle 0| \right) |\alpha\rangle_{a_2} |\beta\rangle_c \\
&= |\alpha\rangle_{a_2} |\beta\rangle_c - e^{-\alpha^2/2} |0\rangle_{a_2} |\beta\rangle_c - e^{-\beta^2/2} |\alpha\rangle_{a_2} |0\rangle_c + e^{-(\alpha^2+\beta^2)/2} |0\rangle_{a_2} |0\rangle_c. \tag{B9}
\end{aligned}$$

This leads to the results

$$\begin{aligned}
\Pi_0^{a_2, c} |\alpha\rangle_{a_2} |0\rangle_c &= \Pi_0^{a_2, c} |0\rangle_{a_2} |\alpha\rangle_c = \text{null} \quad \text{and} \\
\Pi_0^{a_2, c} |\alpha\rangle_{a_2} |-\alpha\rangle_c &= |\alpha\rangle_{a_2} |-\alpha\rangle_c - e^{-\alpha^2/2} |0\rangle_{a_2} |-\alpha\rangle_c - e^{-\alpha^2/2} |\alpha\rangle_{a_2} |0\rangle_c + e^{-\alpha^2} |0\rangle_{a_2} |0\rangle_c. \tag{B10}
\end{aligned}$$

Now, deploying the results of Eq. (B10) in Eq. (B8), we obtain

$$\begin{aligned}
|\psi_0\rangle &= \Pi_0^{a_2,c} |\psi\rangle_{\substack{tot \\ a_1,b_1;b_2' \\ f_a',f_b',g_a',g_c' \\ a_2',c}} \\
&= \frac{1}{2} \left[|00\rangle_{a_1b_1} |0\rangle_{b_2} \left| \sqrt{T'\alpha} \right\rangle_{f_a} \left| \sqrt{T'\alpha} \right\rangle_{f_b} \otimes \left| 2\sqrt{T\eta'_o\alpha} \right\rangle_{g_a} |0\rangle_{g_c} \times \text{null} \right. \\
&\quad + |11\rangle_{a_1b_1} |0\rangle_{b_2} \left| -\sqrt{T'\alpha} \right\rangle_{f_a} \left| -\sqrt{T'\alpha} \right\rangle_{f_b} \otimes |0\rangle_{g_a} \left| -2\sqrt{T\eta'_o\alpha} \right\rangle_{g_c} \times \text{null} \\
&\quad + \left(|01\rangle_{a_1b_1} \left| \sqrt{2T\alpha} \right\rangle_{b_2} \left| \sqrt{T'\alpha} \right\rangle_{f_a} \left| -\sqrt{T'\alpha} \right\rangle_{f_b} + |10\rangle_{a_1b_1} \left| -\sqrt{2T\alpha} \right\rangle_{b_2} \left| -\sqrt{T'\alpha} \right\rangle_{f_a} \left| \sqrt{T'\alpha} \right\rangle_{f_b} \right) \otimes \left| \sqrt{T\eta'_o\alpha} \right\rangle_{g_a} \left| -\sqrt{T\eta'_o\alpha} \right\rangle_{g_c} \otimes \\
&\quad \left(\left| \sqrt{\eta_o T\alpha} \right\rangle_{a_2} \left| -\sqrt{\eta_o T\alpha} \right\rangle_c - e^{-\eta_o T\alpha^2/2} |0\rangle_{a_2} \left| -\sqrt{\eta_o T\alpha} \right\rangle_c - e^{-\eta_o T\alpha^2/2} \left| \sqrt{\eta_o T\alpha} \right\rangle_{a_2} |0\rangle_c + e^{-\eta_o T\alpha^2} |0\rangle_{a_2} |0\rangle_c \right) \\
&= \frac{1}{2} \left(|01\rangle_{a_1b_1} \left| \sqrt{2T\alpha} \right\rangle_{b_2} \left| \sqrt{T'\alpha} \right\rangle_{f_a} \left| -\sqrt{T'\alpha} \right\rangle_{f_b} + |10\rangle_{a_1b_1} \left| -\sqrt{2T\alpha} \right\rangle_{b_2} \left| -\sqrt{T'\alpha} \right\rangle_{f_a} \left| \sqrt{T'\alpha} \right\rangle_{f_b} \right) \otimes \\
&\quad \left| \sqrt{T\eta'_o\alpha} \right\rangle_{g_a} \left| -\sqrt{T\eta'_o\alpha} \right\rangle_{g_c} \otimes |\Psi\rangle_{a_2c}, \tag{B11}
\end{aligned}$$

where

$$|\Psi\rangle_{a_2c} = \left| \sqrt{\eta_o T\alpha} \right\rangle_{a_2} \left| -\sqrt{\eta_o T\alpha} \right\rangle_c - e^{-\eta_o T\alpha^2/2} |0\rangle_{a_2} \left| -\sqrt{\eta_o T\alpha} \right\rangle_c - e^{-\eta_o T\alpha^2/2} \left| \sqrt{\eta_o T\alpha} \right\rangle_{a_2} |0\rangle_c + e^{-\eta_o T\alpha^2} |0\rangle_{a_2} |0\rangle_c. \tag{B12}$$

Now, it can be shown that

$$\begin{aligned}
\text{tr}(|\Psi\rangle_{a_2c} \langle \Psi|) &= \text{tr} \left[\left(\left\langle \sqrt{\eta_o T\alpha} \right| \sqrt{\eta_o T\alpha} \right\rangle_{a_2} \left\langle -\sqrt{\eta_o T\alpha} \right| -\sqrt{\eta_o T\alpha} \right\rangle_c + e^{-\eta_o T\alpha^2} \langle 0|0\rangle_{a_2} \left\langle -\sqrt{\eta_o T\alpha} \right| -\sqrt{\eta_o T\alpha} \right\rangle_c \\
&\quad + e^{-\eta_o T\alpha^2} \left\langle \sqrt{\eta_o T\alpha} \right| \sqrt{\eta_o T\alpha} \right\rangle_{a_2} \langle 0|0\rangle_c + e^{-2\eta_o T\alpha^2} \langle 0|0\rangle_{a_2} \langle 0|0\rangle_c \Big) \\
&\quad + 2 \left(-e^{-\eta_o T\alpha^2/2} \left\langle 0 \right| \sqrt{\eta_o T\alpha} \right\rangle_{a_2} \left\langle -\sqrt{\eta_o T\alpha} \right| -\sqrt{\eta_o T\alpha} \right\rangle_c - e^{-\eta_o T\alpha^2/2} \left\langle \sqrt{\eta_o T\alpha} \right| \sqrt{\eta_o T\alpha} \right\rangle_{a_2} \left\langle 0 \right| -\sqrt{\eta_o T\alpha} \right\rangle_c \\
&\quad + e^{-\eta_o T\alpha^2} \left\langle 0 \right| \sqrt{\eta_o T\alpha} \right\rangle_{a_2} \left\langle 0 \right| -\sqrt{\eta_o T\alpha} \right\rangle_c \Big) + 2 \left(e^{-\eta_o T\alpha^2} \left\langle \sqrt{\eta_o T\alpha} \right| 0 \right\rangle_{a_2} \left\langle 0 \right| -\sqrt{\eta_o T\alpha} \right\rangle_c \\
&\quad - e^{-3\eta_o T\alpha^2/2} \langle 0|0\rangle_{a_2} \left\langle 0 \right| -\sqrt{\eta_o T\alpha} \right\rangle_c \Big) - 2 e^{-3\eta_o T\alpha^2/2} \left\langle 0 \right| \sqrt{\eta_o T\alpha} \right\rangle_{a_2} \langle 0|0\rangle_c \Big] \\
&= \left(1 + e^{-\eta_o T\alpha^2} + e^{-\eta_o T\alpha^2} + e^{-2\eta_o T\alpha^2} \right) + 2 \left(-e^{-\eta_o T\alpha^2} - e^{-\eta_o T\alpha^2} + e^{-2\eta_o T\alpha^2} \right) + 2 \left(e^{-2\eta_o T\alpha^2} - e^{-2\eta_o T\alpha^2} \right) - 2e^{-2\eta_o T\alpha^2} \\
&= 1 - 2e^{-\eta_o T\alpha^2} + e^{-2\eta_o T\alpha^2} = \left(1 - e^{-\eta_o T\alpha^2} \right)^2. \tag{B13}
\end{aligned}$$

Hence,

$$\begin{aligned}
& \text{tr}_{f_a, f_b}^{g_a, g_c}_{a_2, c} \left(|\psi_0\rangle \langle \psi_0| \right) \\
&= \frac{\left(1 - e^{-\eta_o T \alpha^2}\right)^2}{4} \text{tr}_{f_a, f_b} \left[\left(|01\rangle_{a_1 b_1} \langle 01| \otimes |\sqrt{2T}\alpha\rangle_{b_2} \langle \sqrt{2T}\alpha| \otimes |\sqrt{T'}\alpha\rangle_{f_a} \langle \sqrt{T'}\alpha| \otimes |-\sqrt{T'}\alpha\rangle_{f_b} \langle -\sqrt{T'}\alpha| \right. \right. \\
&\quad + |10\rangle_{a_1 b_1} \langle 10| \otimes |-\sqrt{2T}\alpha\rangle_{b_2} \langle -\sqrt{2T}\alpha| \otimes |-\sqrt{T'}\alpha\rangle_{f_a} \langle -\sqrt{T'}\alpha| \otimes |\sqrt{T'}\alpha\rangle_{f_b} \langle \sqrt{T'}\alpha| \\
&\quad + |01\rangle_{a_1 b_1} \langle 10| \otimes |\sqrt{2T}\alpha\rangle_{b_2} \langle -\sqrt{2T}\alpha| \otimes |\sqrt{T'}\alpha\rangle_{f_a} \langle -\sqrt{T'}\alpha| \otimes |-\sqrt{T'}\alpha\rangle_{f_b} \langle \sqrt{T'}\alpha| \\
&\quad \left. \left. + |10\rangle_{a_1 b_1} \langle 01| \otimes |-\sqrt{2T}\alpha\rangle_{b_2} \langle \sqrt{2T}\alpha| \otimes |-\sqrt{T'}\alpha\rangle_{f_a} \langle \sqrt{T'}\alpha| \otimes |\sqrt{T'}\alpha\rangle_{f_b} \langle -\sqrt{T'}\alpha| \right) \right] \\
&\quad \text{tr}_{g_a, g_c} \left[|\sqrt{T}\eta'_o\alpha\rangle_{g_a} \langle \sqrt{T}\eta'_o\alpha| \otimes |-\sqrt{T}\eta'_o\alpha\rangle_{g_c} \langle -\sqrt{T}\eta'_o\alpha| \right] \\
&= \frac{\left(1 - e^{-\eta_o T \alpha^2}\right)^2}{4} \left[|01\rangle_{a_1 b_1} \langle 01| \otimes |\sqrt{2T}\alpha\rangle_{b_2} \langle \sqrt{2T}\alpha| + |10\rangle_{a_1 b_1} \langle 10| \otimes |-\sqrt{2T}\alpha\rangle_{b_2} \langle -\sqrt{2T}\alpha| \right. \\
&\quad \left. + \left(|01\rangle_{a_1 b_1} \langle 10| \otimes |\sqrt{2T}\alpha\rangle_{b_2} \langle -\sqrt{2T}\alpha| + |10\rangle_{a_1 b_1} \langle 01| \otimes |-\sqrt{2T}\alpha\rangle_{b_2} \langle \sqrt{2T}\alpha| \right) e^{-4(1-T)\alpha^2} \right], \tag{B14}
\end{aligned}$$

where $\text{tr}(|\alpha\rangle \langle -\alpha|) = e^{-2\alpha^2}$. The corresponding probability and normalization constant are

$$p_0 = N_0 = \text{tr}_{a_1, b_1} \left[\text{tr}_{f_a, f_b}^{g_a, g_c}_{a_2, c} \left(|\psi_0\rangle \langle \psi_0| \right) \right] = \frac{\left(1 - e^{-\eta_o T \alpha^2}\right)^2}{2}. \tag{B15}$$

This leads to the normalized state

$$\begin{aligned}
\rho_{a_1, b_1, b_2}^0 &= \frac{1}{N_0} \text{tr}_{f_a, f_b}^{g_a, g_c}_{a_2, c} \left(|\psi_0\rangle \langle \psi_0| \right) \\
&= \frac{1}{2} \left[|01\rangle_{a_1 b_1} \langle 01| \otimes |\sqrt{2T}\alpha\rangle_{b_2} \langle \sqrt{2T}\alpha| + |10\rangle_{a_1 b_1} \langle 10| \otimes |-\sqrt{2T}\alpha\rangle_{b_2} \langle -\sqrt{2T}\alpha| \right. \\
&\quad \left. + \left(|01\rangle_{a_1 b_1} \langle 10| \otimes |\sqrt{2T}\alpha\rangle_{b_2} \langle -\sqrt{2T}\alpha| + |10\rangle_{a_1 b_1} \langle 01| \otimes |-\sqrt{2T}\alpha\rangle_{b_2} \langle \sqrt{2T}\alpha| \right) e^{-4(1-T)\alpha^2} \right]. \tag{B16}
\end{aligned}$$

3. State after the homodyne measurement

Charlie now performs the homodyne measurement along the quadrature X_θ on mode b_2 . Here also we consider that the homodyne instruments are not perfect. Rather the efficiency of the homodyne detector is given by η_h . Similar to the earlier cases here also the imperfect homodyne detector could be modeled as a passive beam splitter with transmittivity η_h . Now the action of the imperfect homodyne measurement along quadrature X_θ will lead to the resultant unnormalized state $\rho_{\text{un}}^{\text{hom},0} = \langle X_\theta |_{b_2} \text{tr}_{h_b} \left[(U_{\eta_h}^{h_b, b_2}) \rho_{a_1, b_1; b_2}^0 \otimes |0\rangle_{h_b} \langle 0| (U_{\eta_h}^{h_b, b_2})^\dagger \right] |X_\theta\rangle_{b_2}$ with normalization $N_0^{\text{hom}} = \text{tr}_{a_1, b_1} (\rho_{\text{un}}^{\text{hom},0})$, where X_θ in a mode a is defined as $X_\theta = (ae^{i\theta} + a^\dagger e^{-i\theta})/2$ and with the eigenvalue equation as X_θ defined as $X_\theta |X_\theta\rangle = x_\theta |X_\theta\rangle$.

Thus, after the homodyne measurement by Charlie, the residual normalized state between Alice and Bob will be

$$\rho_{a_1, b_1} = p_0 \frac{\rho_{\text{un}}^{\text{hom},0}}{N_0^{\text{hom}}} = p_0 \rho_{a_1, b_1}^{\text{hom},0}. \tag{B17}$$

In this work we consider the measurement of quadrature operator for the choice of $\theta = \frac{\pi}{2}$, i.e., we consider the *momentum-like* quadrature operator P . Now the measurement of P for a coherent state $|\alpha\rangle$ is $\langle P|\alpha\rangle =$

$$\frac{1}{\pi^{1/4}} e^{-p^2/2} e^{-\alpha^2 - i\sqrt{2}\alpha p}.$$

$$\begin{aligned}
& \text{tr}_{h_b} \left[(U_{\eta_h}^{h_b, b_2}) \rho_{a_1, b_1; b_2}^0 \otimes |0\rangle_{h_b} \langle 0| (U_{\eta_h}^{h_b, b_2})^\dagger \right] \\
&= \frac{1}{2} \text{tr}_{h_b} \left\{ (U_{\eta_h}^{h_b, b_2}) \left[|01\rangle_{a_1 b_1} \langle 01| \otimes |\sqrt{2T}\alpha\rangle_{b_2} \langle \sqrt{2T}\alpha| + |10\rangle_{a_1 b_1} \langle 10| \otimes |-\sqrt{2T}\alpha\rangle_{b_2} \langle -\sqrt{2T}\alpha| \right. \right. \\
&\quad \left. \left. + \left(|01\rangle_{a_1 b_1} \langle 10| \otimes |\sqrt{2T}\alpha\rangle_{b_2} \langle -\sqrt{2T}\alpha| + |10\rangle_{a_1 b_1} \langle 01| \otimes |-\sqrt{2T}\alpha\rangle_{b_2} \langle \sqrt{2T}\alpha| \right) e^{-4(1-T)\alpha^2} \right] \otimes |0\rangle_{h_b} \langle 0| (U_{\eta_h}^{h_b, b_2})^\dagger \right\} \\
&= \frac{1}{2} \text{tr}_{h_b} \left[|01\rangle_{a_1 b_1} \langle 01| \otimes |\sqrt{2T\eta_h}\alpha\rangle_{b_2} \langle \sqrt{2T\eta_h}\alpha| \otimes |\sqrt{2T\eta'_h}\alpha\rangle_{h_b} \langle \sqrt{2T\eta'_h}\alpha| \right. \\
&\quad \left. + |10\rangle_{a_1 b_1} \langle 10| \otimes |-\sqrt{2T\eta_h}\alpha\rangle_{b_2} \langle -\sqrt{2T\eta_h}\alpha| \otimes |-\sqrt{2T\eta'_h}\alpha\rangle_{h_b} \langle -\sqrt{2T\eta'_h}\alpha| \right. \\
&\quad \left. + \left(|01\rangle_{a_1 b_1} \langle 10| \otimes |\sqrt{2T\eta_h}\alpha\rangle_{b_2} \langle -\sqrt{2T\eta_h}\alpha| \otimes |\sqrt{2T\eta'_h}\alpha\rangle_{h_b} \langle -\sqrt{2T\eta'_h}\alpha| \right. \right. \\
&\quad \left. \left. + |10\rangle_{a_1 b_1} \langle 01| \otimes |-\sqrt{2T\eta_h}\alpha\rangle_{b_2} \langle \sqrt{2T\eta_h}\alpha| \otimes |-\sqrt{2T\eta'_h}\alpha\rangle_{h_b} \langle \sqrt{2T\eta'_h}\alpha| \right) e^{-4(1-T)\alpha^2} \right] \\
&= \frac{1}{2} \left[|01\rangle_{a_1 b_1} \langle 01| \otimes |\sqrt{2T\eta_h}\alpha\rangle_{b_2} \langle \sqrt{2T\eta_h}\alpha| + |10\rangle_{a_1 b_1} \langle 10| \otimes |-\sqrt{2T\eta_h}\alpha\rangle_{b_2} \langle -\sqrt{2T\eta_h}\alpha| \right. \\
&\quad \left. + \left(|01\rangle_{a_1 b_1} \langle 10| \otimes |\sqrt{2T\eta_h}\alpha\rangle_{b_2} \langle -\sqrt{2T\eta_h}\alpha| + |10\rangle_{a_1 b_1} \langle 01| \otimes |-\sqrt{2T\eta_h}\alpha\rangle_{b_2} \langle \sqrt{2T\eta_h}\alpha| \right) e^{-4T(1-\eta'_h)\alpha^2} e^{-4(1-T)\alpha^2} \right] \\
&= \frac{1}{2} \left[|01\rangle_{a_1 b_1} \langle 01| \otimes |\sqrt{2T\eta_h}\alpha\rangle_{b_2} \langle \sqrt{2T\eta_h}\alpha| + |10\rangle_{a_1 b_1} \langle 10| \otimes |-\sqrt{2T\eta_h}\alpha\rangle_{b_2} \langle -\sqrt{2T\eta_h}\alpha| \right. \\
&\quad \left. + \left(|01\rangle_{a_1 b_1} \langle 10| \otimes |\sqrt{2T\eta_h}\alpha\rangle_{b_2} \langle -\sqrt{2T\eta_h}\alpha| + |10\rangle_{a_1 b_1} \langle 01| \otimes |-\sqrt{2T\eta_h}\alpha\rangle_{b_2} \langle \sqrt{2T\eta_h}\alpha| \right) e^{-4(1-T\eta_h)\alpha^2} \right], \quad (\text{B18})
\end{aligned}$$

which leads to

$$\begin{aligned}
\rho_{\text{un}}^{\text{hom},0} &= \langle P|_{b_2} \text{tr}_{h_b} \left[(U_{\eta_h}^{h_b, b_2}) \rho_{a_1, b_1; b_2}^0 \otimes |0\rangle_{h_b} \langle 0| (U_{\eta_h}^{h_b, b_2})^\dagger \right] |P\rangle_{b_2} \\
&= \frac{1}{2} \langle P|_{b_2} \left[|01\rangle_{a_1 b_1} \langle 01| \otimes |\sqrt{2T\eta_h}\alpha\rangle_{b_2} \langle \sqrt{2T\eta_h}\alpha| + |10\rangle_{a_1 b_1} \langle 10| \otimes |-\sqrt{2T\eta_h}\alpha\rangle_{b_2} \langle -\sqrt{2T\eta_h}\alpha| \right. \\
&\quad \left. + \left(|01\rangle_{a_1 b_1} \langle 10| \otimes |\sqrt{2T\eta_h}\alpha\rangle_{b_2} \langle -\sqrt{2T\eta_h}\alpha| + |10\rangle_{a_1 b_1} \langle 01| \otimes |-\sqrt{2T\eta_h}\alpha\rangle_{b_2} \langle \sqrt{2T\eta_h}\alpha| \right) e^{-4(1-T\eta_h)\alpha^2} \right] |P\rangle_{b_2} \\
&= \frac{e^{-p^2}}{2\sqrt{\pi}} \left[|01\rangle_{a_1 b_1} \langle 01| e^{-4T\eta_h\alpha^2} + |10\rangle_{a_1 b_1} \langle 10| e^{-4T\eta_h\alpha^2} \right. \\
&\quad \left. + \left(|01\rangle_{a_1 b_1} \langle 10| e^{-4T\eta_h\alpha^2 - 4i\sqrt{T\eta_h}\alpha p} + |10\rangle_{a_1 b_1} \langle 01| e^{-4T\eta_h\alpha^2 + 4i\sqrt{T\eta_h}\alpha p} \right) e^{-4(1-T\eta_h)\alpha^2} \right] \\
&= \frac{e^{-p^2} e^{-4T\eta_h\alpha^2}}{2\sqrt{\pi}} \left[|01\rangle_{a_1 b_1} \langle 01| + |10\rangle_{a_1 b_1} \langle 10| + \left(|01\rangle_{a_1 b_1} \langle 10| e^{-4i\sqrt{T\eta_h}\alpha p} + |10\rangle_{a_1 b_1} \langle 01| e^{4i\sqrt{T\eta_h}\alpha p} \right) e^{-4(1-T\eta_h)\alpha^2} \right], \quad (\text{B19})
\end{aligned}$$

with $N_0^{\text{hom}} = \text{tr}_{a_1, b_1} (\rho_{\text{un}}^{\text{hom},0}) = \frac{e^{-p^2} e^{-4T\eta_h\alpha^2}}{\sqrt{\pi}}$. Therefore,

$$\begin{aligned}
\rho_{a_1, b_1}^{\text{hom},0} &= \frac{\rho_{\text{un}}^{\text{hom},0}}{N_0^{\text{hom}}} \\
&= \frac{1}{2} \left[|01\rangle_{a_1 b_1} \langle 01| + |10\rangle_{a_1 b_1} \langle 10| + \left(|01\rangle_{a_1 b_1} \langle 10| e^{-4i\sqrt{T\eta_h}\alpha p} + |10\rangle_{a_1 b_1} \langle 01| e^{4i\sqrt{T\eta_h}\alpha p} \right) e^{-4(1-T\eta_h)\alpha^2} \right]. \quad (\text{B20})
\end{aligned}$$

Appendix C: Assumptions and secure key rates

1. Assumptions in measurement-device-independent quantum key distribution

In the protocol presented in the main text we have made the following assumptions which conform with those of the measurement-device-independent (MDI) quantum key distribution (QKD) paradigm:

(i) We assume that Alice and Bob have access to secure laboratories. Secure laboratories are assumed to be immune to any side-channel attack since no unwanted system may enter or exit these laboratories. As such, these laboratories should not take part directly in either state preparation or state detection. In the protocol, the DV modes a_1 and b_1 with Alice and Bob, respectively, are assumed to be in these secure laboratories and do not directly take part in the state preparation and transmission. On the other hand, the CV modes a_2 and b_2 are not assumed to be in secure laboratories.

(ii) We also consider a third party, Charlie, who is assumed to be untrusted and can collaborate with an eavesdropper, Eve. In the worst case scenario, we assume that he is identified as Eve herself. The QKD protocol, as described in the main text, dictates that Charlie performs certain measurements and publicly declare the outcomes so that Alice and Bob can share an entangled state. In principle, as an eavesdropper, we assume that Charlie may not perform the operations as dictated by the protocol. However, it is required for him to supply some outcomes to the specified measurements to activate the correlations between Alice and Bob. However, if these outcomes are tampered with or even fabricated, the correlations between Alice and Bob will decrease. It is then possible for Alice and Bob to detect the presence of Eve by various methods including state tomography since the parties know the final state they should potentially share. More details on this assumption and the concept of secure laboratories can be found in Ref. [14].

2. Calculation of the key rates

In this subsection we provide a detailed analysis of the secure keyrate. The secure key rate is evaluated for the final state that Alice and Bob share after Charlie performs the entanglement swapping operation as dictated in the main text. After performing the steps of the protocol, Alice and Bob will share a DV entangled state in modes a_1 and b_1 . The final state is

$$\rho_{a_1 b_1} = \frac{1}{2} \left[|01\rangle \langle 01| + |10\rangle \langle 10| + f \left(g |01\rangle \langle 10| + g^* |10\rangle \langle 01| \right) \right], \quad (\text{C1})$$

where $f = e^{-4(1-T\eta_h)\alpha^2}$, $g = e^{4i\sqrt{T\eta_h}\alpha p}$, g^* is the conjugate of g and p is the result of the homodyne measurement. In the expression of Eq. (C1), the first and second subsystems correspond to modes a_1 and b_1 with Alice and Bob, respectively. Since the outcome Π_0 for the projective measurement occurs with non-unit probability, Alice and Bob share the state $\rho_{a_1 b_1}$ with probability (See Sec B 2 for a detailed derivation),

$$p_0 = \frac{\left(1 - e^{-\eta_o T \alpha^2}\right)^2}{2}. \quad (\text{C2})$$

In order to evaluate the secure keyrate, we assume the existence of an eavesdropper Eve with system E . We assume that Eve can potentially collaborate with the untrusted party Charlie while also having access to the two quantum channels which are used to transmit the CV systems.

The secure key rate r between Alice and Bob is

$$r \geq p_0 [I(A : B) - \chi(A : E)], \quad (\text{C3})$$

where we have multiplied the expression with the probability of sharing the final resource.

Evaluating the mutual information between Alice and Bob is relatively simple and is accomplished by using their observed joint statistics. We consider that Alice and Bob choose the observable σ_Z to perform their measurements on the state $\rho_{a_1 b_1}$. In this case we obtain $I(A : B) = 1$ bit.

In order to evaluate the Holevo bound, we assume that Eve has access to a purification of the state $\rho_{a_1 b_1}$, which we denote by $\rho_{a_1 b_1 E}$, such that $\rho_E = \text{tr}_{a_1 b_1}(\rho_{a_1 b_1 E})$ is the reduced state of Eve. Moreover, we also assume that Alice's measurement outcomes are represented by rank-1 operators. Since $\rho_{a_1 b_1 E}$ is pure by definition, we have $S(\rho_{a_1 b_1}) = S(\rho_E)$, where $S(X)$ is the Von Neumann entropy of a system X .

Moreover, if Alice's measurement outcomes are represented by rank-1 operators, then the reduced state of Bob and Eve conditioned on Alice's outcome x , given by $\rho_{b_1 E}(x)$, is also pure. Therefore, by definition of Von Neumann

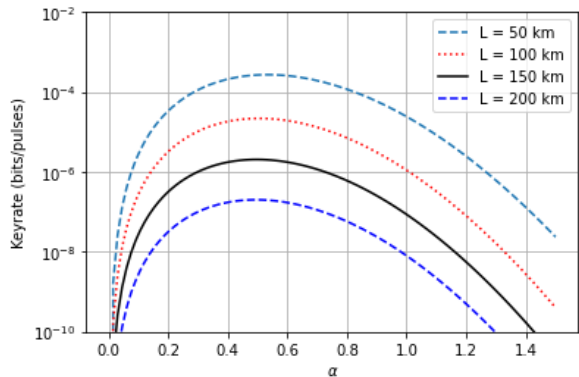


FIG. 4. Secure key rate as a function of the coherent amplitude α for different values of transmission distance. We fix the channel loss at $l = 0.2$ dB/km, which corresponds to losses in standard optical fibres. The value of α which maximizes the key rate is found to be the same in each case.

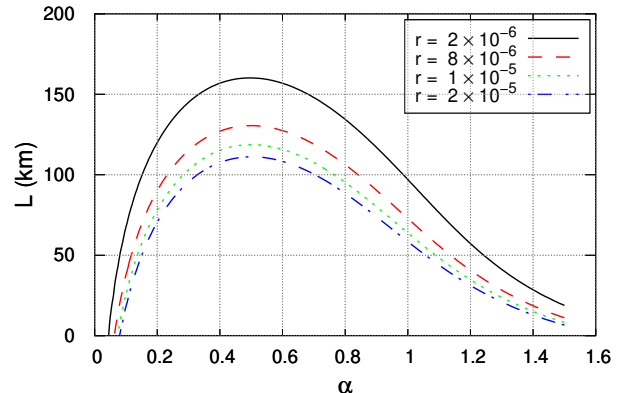


FIG. 5. The total transmission distance as a function of the coherent amplitude for different values of the secure key rate. We fix the channel loss at $l = 0.2$ dB/km which corresponds to losses in standard optical fibres. The optimal value of α which maximizes the transmission distance is found to be the same in each case. The unit for the secure key rate r is bits/pulse.

entropy, we have $S(\rho_E(x)) = S(\rho_{b_1}(x))$. The Holevo bound can then be written as [14]

$$\begin{aligned} \chi(A : E) &= S(\rho_{a_1 b_1}) - \sum_x p(x) S(\rho_{b_1}(x)) \\ &= S(\rho_{a_1 b_1}), \end{aligned} \quad (\text{C4})$$

where for the last equality we have used the fact that $S(\rho_{b_1}(x)) = 0$ for all outcomes x of Alice for the observable σ_Z by construction of the state in Eq. (C1).

Therefore, the final form of the secure key rate can be written as

$$r \geq p_0 [1 - S(\rho_{a_1 b_1})], \quad (\text{C5})$$

where, because of the construction of the final state, the secure key rate is only a function of its von Neumann entropy. It should be noted that the state itself is a function of the detection efficiencies η_h and η_0 , the result of the homodyne measurement p , the coherent amplitude α , and the transmission coefficient T .

Generally, for an experimental realization of the QKD protocol, the labs of Alice and Bob are fixed at some distance L . While in the main text we show how the secure key rate behaves with varying L , there is another important parameter that we keep fixed. The key rate is also a function of the coherent amplitude α . As seen in the main text, α cannot be chosen arbitrarily, as there exists an optimal value which can either maximize the key rate or the total transmission distance. In Fig. 4, we plot the secure key rate as a function of the coherent amplitude for a fixed value of the transmission distance. We see that there exists an optimal value $\alpha \approx 0.5$ which maximizes the total secure key rate for any value of transmission distance. Coincidentally, we find that the same value also maximizes the total transmission distance for fixed value of secure key rate as seen in Fig. 5. Therefore, this is the value of α that we use in the main text to show the security of our protocol.

Appendix D: Logarithmic negativity of hybrid entangled states undergoing photon loss

In our protocol we use the CV part of the HE state for transmission via a lossy quantum channel. It can be shown that under photon losses in the CV part, an HE state can still retain correlations for a particular value of α .

We analyse the amount of correlations that a HE state retains after its CV system is transmitted via a lossy quantum channel. Upon transmission the CV part undergoes photon loss which is directly dependent on the value of α chosen. We show that the correlations in a HE state after its CV part has undergone transmission loss is a non-monotonic function of its coherent amplitude. Specifically, we evaluate the logarithmic negativity [53, 68] of the

initial HE state as a function of transmission loss. We find that for $\alpha \approx 0.5$, the HE state is highly robust against noise.

Let us consider the HE state

$$|\psi\rangle_{ab} = \frac{1}{\sqrt{2}} \left(|0\rangle_a |\alpha\rangle_b + |1\rangle_a |-\alpha\rangle_b \right). \quad (\text{D1})$$

Suppose that the mode b undergoes photon loss. The process of photon loss can be equivalently modeled as passage through a beam splitter with reflectivity R ($0 \leq R \leq 1$) while the other input to the beam splitter is taken to be vacuum. In such a case, the beam splitter matrix is $\begin{pmatrix} \sqrt{1-R} & \sqrt{R} \\ -\sqrt{R} & \sqrt{1-R} \end{pmatrix}$, where $R = 0$ and $R = 1$ stand for zero photon loss and complete photon loss, respectively. To that end, let us consider that the mode b passes through such a beam splitter while the other input is at $|0\rangle$ in mode c . As a consequence, the total state after passage through the beam splitter becomes

$$|\psi\rangle_{ab} \otimes |0\rangle_c \xrightarrow{\text{bs}} \frac{1}{\sqrt{2}} \left(|0\rangle_a \left| \sqrt{1-R\alpha} \right\rangle_b \left| \sqrt{R\alpha} \right\rangle_c + |1\rangle_a \left| -\sqrt{1-R\alpha} \right\rangle_b \left| -\sqrt{R\alpha} \right\rangle_c \right). \quad (\text{D2})$$

Subsequently, the two-mode state in modes a and b after photon loss is obtained by tracing over the ancillary mode c as

$$\begin{aligned} \rho_{ab}^{\text{loss}} &= \text{tr}_c \left[\frac{1}{2} \left(\left| 0, \sqrt{1-R\alpha} \right\rangle_{ab} \left\langle 0, \sqrt{1-R\alpha} \right| \otimes \left| \sqrt{R\alpha} \right\rangle_c \left\langle \sqrt{R\alpha} \right| + \left| 1, -\sqrt{1-R\alpha} \right\rangle_{ab} \left\langle 1, -\sqrt{1-R\alpha} \right| \otimes \left| -\sqrt{R\alpha} \right\rangle_c \left\langle -\sqrt{R\alpha} \right| \right. \right. \\ &\quad \left. \left. + \left| 0, \sqrt{1-R\alpha} \right\rangle_{ab} \left\langle 1, -\sqrt{1-R\alpha} \right| \otimes \left| \sqrt{R\alpha} \right\rangle_c \left\langle -\sqrt{R\alpha} \right| + \left| 1, -\sqrt{1-R\alpha} \right\rangle_{ab} \left\langle 0, \sqrt{1-R\alpha} \right| \otimes \left| -\sqrt{R\alpha} \right\rangle_c \left\langle \sqrt{R\alpha} \right| \right) \right] \\ &= \frac{1}{2} \left(\left| 0, \sqrt{1-R\alpha} \right\rangle_{ab} \left\langle 0, \sqrt{1-R\alpha} \right| + \left| 1, -\sqrt{1-R\alpha} \right\rangle_{ab} \left\langle 1, -\sqrt{1-R\alpha} \right| + e^{-2R\alpha^2} \left| 0, \sqrt{1-R\alpha} \right\rangle_{ab} \left\langle 1, -\sqrt{1-R\alpha} \right| \right. \\ &\quad \left. + e^{-2R\alpha^2} \left| 1, -\sqrt{1-R\alpha} \right\rangle_{ab} \left\langle 0, \sqrt{1-R\alpha} \right| \right) \\ &= \frac{1}{2} \left[|0\rangle_a \langle 0| \otimes \left| \sqrt{1-R\alpha} \right\rangle_b \left\langle \sqrt{1-R\alpha} \right| + |1\rangle_a \langle 1| \otimes \left| -\sqrt{1-R\alpha} \right\rangle_b \left\langle -\sqrt{1-R\alpha} \right| \right. \\ &\quad \left. + e^{-2R\alpha^2} \left(|0\rangle_a \langle 1| \otimes \left| \sqrt{1-R\alpha} \right\rangle_b \left\langle -\sqrt{1-R\alpha} \right| + |1\rangle_a \langle 0| \otimes \left| -\sqrt{1-R\alpha} \right\rangle_b \left\langle \sqrt{1-R\alpha} \right| \right) \right]. \quad (\text{D3}) \end{aligned}$$

In order to evaluate the entanglement content in this state, we use logarithmic negativity as a measure of entanglement. For a bipartite state ρ_{ab}^{loss} it is defined as $E_N(\rho_{ab}^{\text{loss}}) = \log_2 \left\| \left(\rho_{ab}^{\text{loss}} \right)^{\text{P.T.}} \right\|_1$, where $\|\cdot\|_1$ is the trace norm and P.T. stands for partial transpose over any one of the modes a or b . We evaluate the logarithmic negativity for the state after photon loss in Eq. (D3) numerically and is shown in the main text.